Horizontal Drying Fronts During Solvent Evaporation from Latex Films

Alexander F. Routh and William B. Russel
Dept. of Chemical Engineering, Princeton University, Princeton, NJ 08544

Latex films cast on a substrate often dry nonuniformly, with a drying front separating fluid domains from solidified regions passing across the film. For initial film thicknesses that are smaller than the characteristic horizontal distance, the analysis predicts surface-tension-driven horizontal flow. In a limit that ensures vertical homogeneity it is shown how a front of close-packed particles forms and propagates. Imposing a maximum for the capillary pressure causes a solvent front to recede into the film. This recession is minimal, but can markedly affect the propagation of the particle front. An overall mass balance offers a solution for infinite capillary pressure, thereby illustrating the mechanism for propagation of the front. The positions of the fronts are predicted for both infinite and finite domains as a function of the maximum capillary pressure. Selective or nonuniform evaporation produces final film profiles, while the evaporating regions are still visible. After predictions over different size areas are made, the smallest area is compared with experiment.

Introduction

The problem of film formation has been considered in the literature for over 50 years (Brown, 1956; Henson et al., 1953; Sheetz, 1965; Vanderhoff et al., 1966; Winnik, 1997; Dobler and Holl, 1996). The accepted mechanism consists of three stages. Evaporation from an initially fluid dispersion leads to concentration of the particles into a close-packed array. Further evaporation along with deformation of the particles eliminates voids, although the original particles remain distinguishable. Finally, diffusion of polymer across the interfaces between particles leads to a structure with mechanical integrity and with the individual particles no longer distinguishable.

The second step in this mechanism, which considers deformation of the individual particles, is the most contentious. Four major methods for deformation have been proposed. Two depend on the deformation of viscous spheres as described by Frenkel (1945), as a balance between the work done by surface tension against viscous dissipation inside the particles: wet sintering driven by the polymer–water interfacial tension (Vanderhoff et al., 1966) and dry sintering (Dillon et al., 1951) driven by the polymer–air interfacial tension. Brown (1956) considered the dominant mechanism to be the elastic deformation of the particles driven by capillary pressure due to the water–air surface tension. The fourth deformation mechanism is due to Sheetz (1965). Here capillary forces deform a surface layer of particles by Brown's method, and the subsequent flow of evaporating water, through this layer, causes a compressive force to deform the particles below.

The first stage in the film formation process, evaporation of water to bring the particles into close packing, has been less contentious. While the process is generally considered to be spatially uniform, Sheetz (1965) reported a drying front, as did Croll (1986). Winnik and Feng (1996) proposed a drying process (Figure 1), in which lateral flow of fluid due to evaporation from a dry edge propagates such a region into the remaining dispersion. They noted that dispersions of soft latexes dry more slowly than dispersions of hard latexes, while mixtures of hard and soft latexes dry more slowly still. Here soft latexes presumably deform elastically and quickly under capillary forces (i.e., by Brown's method), while hard latexes resist deformation. Winnik and Feng attribute the driving force for the front propagation to preferential drying at the "dry/wet boundary," which will be considered further later. Eckersley and Rudin (1990) argue that any moving front will affect the deformation mechanism experienced by the particles during compaction.

Correspondence concerning this article should be addressed to W. B. Russel.

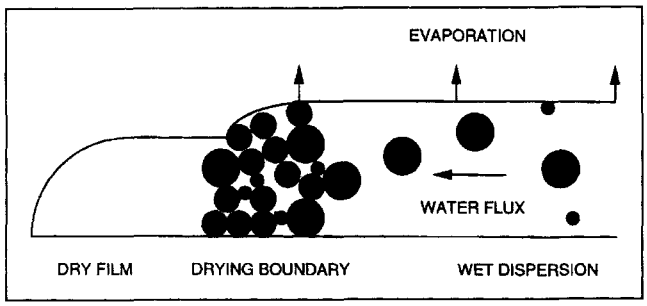

Figure 1. Conceptual view of the drying mechanism.
Adapted from Winnik and Feng (1996).

There has been much work on the flow of dispersions relevant to the drying process. The analysis of Overdiep (1986a, b) links gradients in surface tension caused by evaporation to leveling of a sinusoidally rippled surface. Wilson (1993) assumes surface tension and viscosity to be linear functions of solute concentration and predicts the surface of a sinusoidally perturbed fluid to oscillate with a decaying amplitude. Deegan et al. (1997) consider evaporation from a liquid drop—for example, a coffee drop—and predict the formation of deposits of dispersed solids at the edge. The preceding analyses invoke the lubrication approximation with flow driven by surface tension. Teletzke et al. (1987) derive the equations for the evolution of the film height in the absence of evaporation but with gradients in surface tension. The major controversy over the resulting equation resides in the boundary condition at the edge of the film. Bertozzi (1996) discusses how a no-slip boundary condition at the edge of the film leads to an infinite stress at the corner of the film, which can be removed with a slip boundary condition. For a review of thin-film flows, see Oron et al. (1997).

In this article, we develop a theory based on the lubrication approximation that captures this drying front, while ignoring particle deformation. The stress singularity at the edge of the film is avoided by a scaling argument that leads to a particularly simple form for the fluid equations. The position of the front of close-packed particles is tracked and the effect of solvent recession into the film investigated. Nonuniform evaporation from an initially uniform dispersion is considered with the profile of such films shown over different lengths. This is then compared to some experimental observations on films dried in a nonuniform fashion.

Model

For a stable dispersion as shown in Figure 2, the local solids fraction ϕ satisfies a conservation equation

$$\frac{\partial \phi}{\partial t} + \nabla \cdot \phi \boldsymbol{U} = \boldsymbol{0}, \tag{1}$$

where $\boldsymbol{U}$ is the particle velocity relative to fixed coordinates. Particles of radius a in a fluid of viscosity μ move due to fluid motion and other forces according to

$$\boldsymbol{U} = \boldsymbol{u} + \frac{K(\phi)}{6\pi\mu a}(\boldsymbol{F} - \nabla\mu'), \tag{2}$$

with $\boldsymbol{u}$ the volume-averaged velocity of the dispersion, $\boldsymbol{F}$ the total external force acting on the particles, $\nabla\mu'$ the gradient in the chemical potential, and $K(\phi)$ the dimensionless collective mobility, accounting for the hydrodynamic interactions among the spheres.

The chemical potential is given by

$$\mu' = \mu'_p - \frac{4\pi a^3}{3\nu_s}\mu'_s \tag{3}$$

with μ'_s and μ'_p the chemical potentials of the solvent and particles, respectively, and ν_s the volume of a water molecule. The osmotic pressure Π is related to the chemical potential and vapor pressure, p_{vap}, of the solvent through

$$\Pi = -\frac{\mu'_s - \mu'^0_s}{\nu_s} = -\frac{k_b T}{\nu_s}\ln\frac{p_{\text{vap}}}{p^0_{\text{vap}}} \equiv \frac{3k_b T}{4\pi a^3}\phi Z(\phi), \tag{4}$$

where k_b is Boltzmann's constant and p^0_{vap} and μ'^0_s are a reference vapor pressure and chemical potential, respectively. Interactions between particles in the dispersion determine the compressibility factor $Z(\phi)$. With the Gibbs Duhem equation

$$n\nabla\mu'_p + n_s\nabla\mu'_s = 0, \tag{5}$$

where n is the number density of particles, and n_s is the number density of solvent molecules, the flux for particles under negligible external force becomes

$$\phi\boldsymbol{U} = \phi\boldsymbol{u} - D_o K(\phi)\frac{d(\phi Z(\phi))}{d\phi}\nabla\phi, \tag{6}$$

where $D_o = k_b T/6\pi\mu a$. Substituting this into Eq. 1 yields the particle-conservation equation

$$\frac{\partial \phi}{\partial t} + \nabla\cdot\phi\boldsymbol{u} = \nabla\cdot D_o K(\phi)\frac{d[\phi Z(\phi)]}{d\phi}\nabla\phi, \tag{7}$$

which, along with overall momentum and volume conservation expressions,

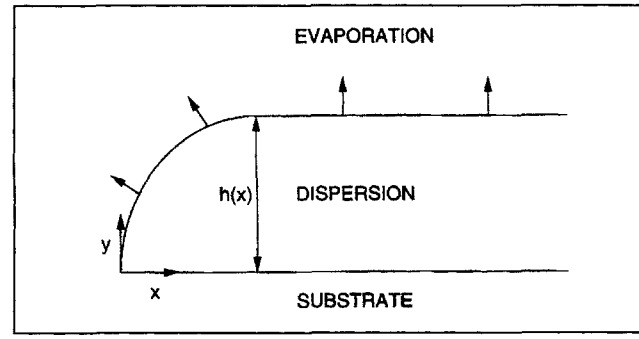

Figure 2. Evaporation from a film spread on a substrate.

$$\eta_0 \nabla^2 \boldsymbol{u} = \nabla(p + \Pi) \tag{8}$$

$$\nabla \cdot \boldsymbol{u} = 0, \tag{9}$$

where η_0 is the low shear viscosity of the dispersion, describes the fluid mechanics.

The evaporation rate from the free surface is controlled by convective mass transfer and, if required, diffusion from the water surface to the edge of the film, so that

$$\dot{E} = \frac{\nu_s(p_{\text{vap}} - p^{\infty}_{\text{vap}})}{k_b T\left(\frac{1}{k} + \frac{S}{D_{\text{vap}}}\right)}, \tag{10}$$

where p^{∞}_{vap} is the vapor pressure in the bulk; D_{vap} is the diffusion coefficient of vapor through the packed bed; k is the gas phase mass-transfer coefficient; and S is the distance through which any vapor must diffuse. Therefore, for early stages when the water surface is coincident with the surface of the film, Eq. 4 yields

$$\dot{E} = \frac{\nu_s k}{k_b T}\left\{p^0_{\text{vap}} \exp\left[-\frac{3\nu_s}{4\pi a^3}\phi Z(\phi)\right] - p^{\infty}_{\text{vap}}\right\}. \tag{11}$$

Since $\nu_s \ll 4\pi a^3/3$, the evaporation rate only depends on the relative humidity and temperature.

Scaling and Lubrication Approximation

Scaling vertical distances on the initial film height, H, horizontal distances on a yet to be defined distance, L, vertical velocities on the evaporation rate, $\dot{E}$, and by continuity, horizontal velocities on $L\dot{E}/H$, yields the characteristic time as $H/\dot{E}$, and the characteristic pressure as $\eta_0 \dot{E} L^2/H^3$, as well as the following set of equations:

$$\frac{6\pi\mu a H\dot{E}}{k_b T}\left[\frac{\partial \phi}{\partial \bar{t}} + \frac{\partial \phi \bar{u}_x}{\partial \bar{x}} + \frac{\partial \phi \bar{u}_y}{\partial \bar{y}}\right] = \frac{H^2}{L^2}\frac{\partial}{\partial \bar{x}}\left[K(\phi)\frac{d(\phi Z(\phi))}{d\phi}\frac{\partial \phi}{\partial \bar{x}}\right] + \frac{\partial}{\partial \bar{y}}\left[K(\phi)\frac{d(\phi Z(\phi))}{d\phi}\frac{\partial \phi}{\partial \bar{y}}\right] \tag{12}$$

$$\frac{\partial \bar{u}_x}{\partial \bar{x}} + \frac{\partial \bar{u}_y}{\partial \bar{y}} = 0 \tag{13}$$

$$\frac{\partial(\bar{p} + \bar{\Pi})}{\partial \bar{x}} = \frac{H^2}{L^2}\frac{\partial^2 \bar{u}_x}{\partial \bar{x}^2} + \frac{\partial^2 \bar{u}_x}{\partial \bar{y}^2} \tag{14}$$

$$\frac{\partial(\bar{p} + \bar{\Pi})}{\partial \bar{y}} = \frac{H^4}{L^4}\frac{\partial^2 \bar{u}_y}{\partial \bar{x}^2} + \frac{H^2}{L^2}\frac{\partial^2 \bar{u}_y}{\partial \bar{y}^2}. \tag{15}$$

Boundary conditions are zero vertical and horizontal velocity at the substrate, zero horizontal velocity as $\bar{x} \to \infty$ and at $\bar{x} = 0$, as well as zero flux of particles and zero tangential traction at the moving top boundary of the film, $\bar{y} = \bar{h}(\bar{x}, \bar{t})$. The pressure at the free surface is given by the surface tension of the dispersion and the curvature of the surface at that point. We also know that $\phi \to \phi_0/(1 - \bar{t})$ as $\bar{x} \to \infty$, since this represents the one-dimensional film that merely responds to evaporation and decreases linearly and evenly with time.

With the lubrication approximation that $H^2/L^2 \ll 1$ we find that $(\bar{p} + \bar{\Pi}) \neq f(\bar{y})$ where f is any function. Therefore the local curvature, κ, of the surface

$$\kappa = \frac{\partial}{\partial x}\left(-\frac{\partial h/\partial x}{\sqrt{1 + (\partial h/\partial x)^2}}\right) = -\frac{H}{L^2}\left(\frac{\partial^2 \bar{h}}{\partial \bar{x}^2}\right) \tag{16}$$

determines the total pressure locally in the film as

$$\bar{p} + \bar{\Pi} = \frac{-H^4 \gamma}{\eta_0 \dot{E} L^4}\left(\frac{\partial^2 \bar{h}}{\partial \bar{x}^2}\right), \tag{17}$$

where γ is the surface tension of the dispersion. Substituting into Eq. 14, integrating, and applying the no-slip condition at $\bar{y} = 0$ as well as zero shear at the free surface determines the transverse velocity as

$$\bar{u}_x = \frac{H^4 \gamma}{\eta_0 \dot{E} L^4}\left[\frac{\partial^3 \bar{h}}{\partial \bar{x}^3}\bar{h}\bar{y} - \frac{1}{2}\frac{\partial^3 \bar{h}}{\partial \bar{x}^3}\bar{y}^2\right]. \tag{18}$$

Integration of Eq. 13 in the vertical direction, and noting that continuity of flux at the top interface sets $\bar{u}_y(\bar{h}) = 1 + \partial \bar{h}/\partial \bar{t} + \bar{u}_x(\bar{h})\partial \bar{h}/\partial \bar{x}$ within the lubrication approximation, gives, after substitution of Eq. 18, the following partial differential equation for $\bar{h}$

$$1 + \frac{\partial \bar{h}}{\partial \bar{t}} + \frac{H^4 \gamma}{3\eta_0 \dot{E} L^4}\left[\bar{h}^3 \frac{\partial^4 \bar{h}}{\partial \bar{x}^4} + 3\bar{h}^2 \frac{\partial \bar{h}}{\partial \bar{x}}\frac{\partial^3 \bar{h}}{\partial \bar{x}^3}\right] = 0. \tag{19}$$

Setting $H^4\gamma/3\eta_0 \dot{E} L^4 = 1$ to balance the flow due to surface tension with that caused by evaporation determines the previously undefined length scale L and leaves our equation for the film height,

$$1 + \frac{\partial \bar{h}}{\partial \bar{t}} + \frac{\partial}{\partial \bar{x}}\left(\bar{h}^3 \frac{\partial^3 \bar{h}}{\partial \bar{x}^3}\right) = 0. \tag{20}$$

Estimating γ as 0.073 N/m, η_0 as 1 Ns/m^2, and $\dot{E}$ as 0.3 cm per day (Keddie et al., 1995) yields $H^2/L^2 \approx 1.2 \times 10^{-3}$, which suggests the lubrication approximation to be reasonable.

The boundary conditions on Eq. 20 are

$$\bar{h} = 0, \qquad \bar{x} = 0 \tag{21}$$

$$\frac{\partial \bar{h}}{\partial \bar{x}} = 0, \qquad \bar{x} \to \infty \tag{22}$$

$$\bar{h} \to 1 - \bar{t}, \qquad \bar{x} \to \infty \tag{23}$$

plus a fourth boundary condition derived explicitly below. The initial condition is obviously arbitrary. We generally adopt

$\bar{h} = 1$ for $\bar{x} > 0$, although a circular arc at the lefthand edge of the film produces qualitatively similar results.

The natural boundary condition at the edge of the film is specification of a contact angle, θ, determined by the fluid, substrate, and surrounding atmosphere as $\partial h/\partial x = \tan\ \theta$. This, however, renders the equations inhomogeneous, and after scaling becomes

$$\frac{\partial \bar{h}}{\partial \bar{x}} = \frac{L}{H}\tan\theta \gg 1. \tag{24}$$

Applying Eq. 20 at $\bar{x} = 0$, differentiating with respect to $\bar{x}$ to obtain

$$\frac{\partial}{\partial \bar{t}}\frac{\partial \bar{h}}{\partial \bar{x}} + 6\bar{h}\left(\frac{\partial \bar{h}}{\partial \bar{x}}\right)^2\frac{\partial^3 \bar{h}}{\partial \bar{x}^3} + 3\bar{h}^2\frac{\partial^2 \bar{h}}{\partial \bar{x}^2}\frac{\partial^3 \bar{h}}{\partial \bar{x}^3} + 6\bar{h}^2\frac{\partial \bar{h}}{\partial \bar{x}}\frac{\partial^4 \bar{h}}{\partial \bar{x}^4} + \bar{h}^3\frac{\partial^5 \bar{h}}{\partial \bar{x}^5} = 0, \tag{25}$$

and noting that $\bar{h} = 0$ at $\bar{x} = 0$, leaves

$$\frac{\partial}{\partial \bar{t}}\frac{\partial \bar{h}}{\partial \bar{x}} = 0, \tag{26}$$

implying that the contact angle, when viewed from an outer region, remains constant at its initial value.

Differentiating Eq. 25 again and neglecting any term containing $\bar{h}$ determines

$$\frac{\partial}{\partial \bar{t}}\frac{\partial^2 \bar{h}}{\partial^2 \bar{x}} + 6\left(\frac{\partial \bar{h}}{\partial \bar{x}}\right)^3\frac{\partial^3 \bar{h}}{\partial \bar{x}^3} = 0, \tag{27}$$

which with Eq. 24 sets

$$\frac{\partial^3 \bar{h}}{\partial \bar{x}^3} = -\frac{1}{6\tan^3\theta}\left(\frac{H}{L}\right)^3\frac{\partial}{\partial \bar{t}}\frac{\partial^2 \bar{h}}{\partial^2 \bar{x}}. \tag{28}$$

Therefore, by the scaling, the third derivative is negligible to $O(H/L)$ at $\bar{x} = 0$.

Convection without Evaporation

In Eq. 20 spatial derivatives represent flow resulting from curvature imposed on the film, and the term of unity is from the evaporation reducing the film size. Neglecting evaporation and concentrating on the curvature-induced flow leaves

$$\frac{\partial \bar{h}}{\partial t} + \frac{\partial}{\partial \bar{x}}\left(\bar{h}^3\frac{\partial^3 \bar{h}}{\partial \bar{x}^3}\right) = 0. \tag{29}$$

We expect a similarity solution, since introducing $\eta = \bar{x}/\bar{t}^{1/4}$ reduces the PDE to the ODE,

$$\frac{d}{d\eta}\left(\bar{h}^3\frac{d^3 \bar{h}}{d\eta^3}\right) = \frac{1}{4}\eta\frac{d\bar{h}}{d\eta}, \tag{30}$$

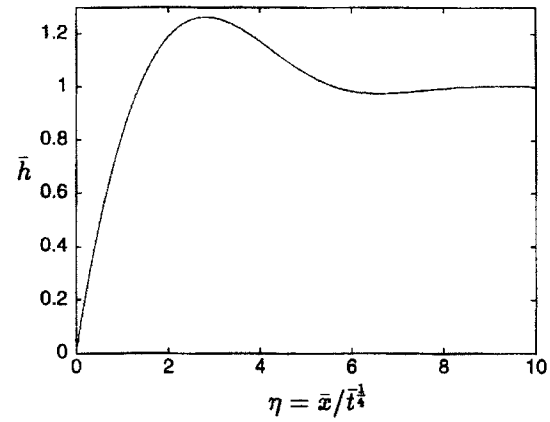

Figure 3. Similarity solution without evaporation.

with the boundary conditions collapsing to

$$\bar{h} \to 0, \qquad \eta \to 0 \tag{31}$$

$$\frac{d^3 \bar{h}}{d\eta^3} \to 0, \qquad \eta \to 0 \tag{32}$$

$$\bar{h} \to 1, \qquad \eta \to \infty \tag{33}$$

$$\frac{d\bar{h}}{d\eta} \to 0, \qquad \eta \to \infty. \tag{34}$$

Solution by a shooting method with a Runge-Kutta scheme, with iteration on $d\bar{h}/d\eta$ and $d^2\bar{h}/d\eta^2$ at $\eta = 0$ to satisfy the boundary conditions as $\eta \to \infty$, results in the self-similar profile in Figure 3. Note that flow driven by the curvature-induced pressure reduces the film height up to $\eta = 1$, and results in accumulation of material above the initial height up to $\eta = 4$. For $\eta > 8$, the fluid is unaffected by the initially square shape.

Convection with Evaporation

Reintroducing evaporation requires a numerical method for solving partial differential equations. Finite differencing Eq. 20 leads to

$$\frac{\partial \bar{h}_i}{\partial \bar{t}} = -\frac{1}{\Delta \bar{x}^4}\left(\Delta \bar{x}^4 + \frac{3}{4}\bar{h}_i^2\left[\bar{h}_{i+1} - \bar{h}_{i-1}\right] \times \left[\bar{h}_{i+2} - 2\bar{h}_{i+1} + 2\bar{h}_{i-1} - \bar{h}_{i-2}\right] + \bar{h}_i^3\left[\bar{h}_{i+2} - 4\bar{h}_{i+1} + 6\bar{h}_i - 4\bar{h}_{i-1} + \bar{h}_{i-2}\right]\right), \tag{35}$$

where the subscript refers to spatial position. This can then be solved using a fourth-order Runge-Kutta scheme to step forward in time. To check the accuracy we removed the evaporation term from Eq. 35 and ran to $\bar{t} = 1$ to obtain a curve that coincides with the similarity solution (Figure 3).

Curves with evaporation (Figure 4) show a peak due to accumulation of material driven from the initially square edge as surface tension forces the shape toward a circle. At early

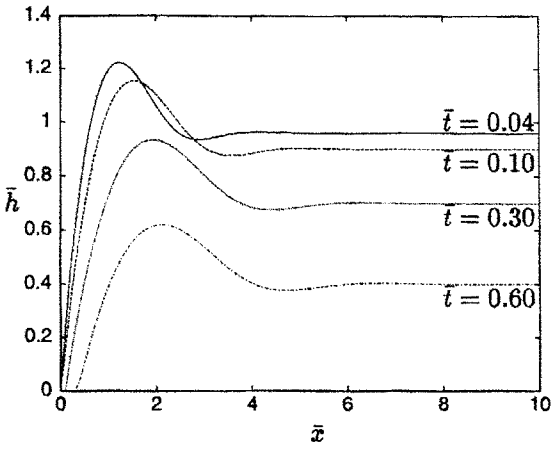

Figure 4. Evolution of height of film with time for $\bar{t} = 0.04$ (—); 0.10 (– –); 0.30 (...); and 0.60 (– · –).

times the flow is dominated by surface tension, and the boundary condition of zero third derivative at the edge of the film seems reasonable. The slope of the film surface at the edge of the film remains constant as dictated by Eq. 26, and the shape of the surface resembles that from the similarity solution. At later times the surface away from the edge follows the similarity solution, suggesting that surface tension still dominates the shape. The edge of the film, however, has moved from $\bar{x} = 0$ as all the fluid evaporates, so our boundary conditions at $\bar{x} = 0$ become invalid. Evaporation reduces the overall magnitude evenly over the entire domain, and at a great distance the height asymptotes to $1 - \bar{t}$ as expected. When we include particles, the accumulation of material at the edge, as seen by Deegan et al. (1997), will hold the edge of the film at $\bar{x} = 0$, making solutions shown here at the later times irrelevant. The boundary conditions at $\bar{x} = 0$ are then replaced by conditions on the flux at the edge of the fluid region.

Drying Fronts

Infinite capillary pressure

So far the particles have been ignored, though the volume fraction follows from Eq. 12. With the lubrication approximation, the dimensionless group $6\pi\mu a H\dot{E}/k_bT$, which is the rate of evaporation divided by the rate of diffusion, controls the vertical transport of particles. If small, ϕ varies little in the vertical direction. We therefore have effectively a zero Peclet number in the vertical direction and an infinite horizontal Peclet number, since horizontal diffusion is small within the lubrication approximation. Scaling the zero flux condition at the top surface

$$\phi\frac{\partial h}{\partial t} = \phi u_y(h) - \frac{k_bT}{6\pi\mu a}K(\phi)\frac{d(\phi Z)}{d\phi}\frac{\partial\phi}{\partial y} - \phi u_x(h)\frac{\partial h}{\partial x}, \tag{36}$$

and integrating Eq. 12 over the film thickness yields

$$\frac{\partial\bar{h}\phi}{\partial\bar{t}} + \frac{\partial\phi\bar{h}\tilde{\bar{u}}_x}{\partial\bar{x}} = 0, \tag{37}$$

where $\tilde{\bar{u}}_x$ is the dimensionless vertically averaged horizontal velocity, obtained from Eq. 18 as

$$\tilde{\bar{u}}_x = \bar{h}^2\frac{\partial^3\bar{h}}{\partial\bar{x}^3}. \tag{38}$$

Here we set the initial condition as $\phi = 0.4$ and integrate Eq. 37 in parallel with Eq. 20, assuming the viscosity of the dispersion to be constant until the local volume fraction reaches the fluid–solid transition, where the viscosity becomes infinite and the height of the film is fixed. This transition lies in the range $0.52 < \phi < 0.74$, assuming that the particles do not yet deform. Some previous work has assumed $\phi_m = 0.74$, which corresponds to a face-centered cubic structure, whereas $\phi_m = 0.52$ corresponds to a simple cubic packing. Here we assume random close packing at $\phi_m = 0.64$. The actual value should depend on the rate of evaporation, which determines whether the particles have time to make the preferred disorder–order transition (Russel, 1990).

At the position of the fluid–solid transition, a particle balance

$$\frac{d\bar{x}_f}{d\bar{t}} = -\frac{\phi(\bar{x}_f^+)\tilde{\bar{u}}_x(\bar{x}_f^+)}{\phi_m - \phi(\bar{x}_f^+)} \tag{39}$$

relates $\bar{x}_f$, the position of the particle front, to conditions beyond the front ($\bar{x}_f^+$). A water balance across the front yields

$$\frac{d\bar{x}_f}{d\bar{t}} = \frac{\tilde{\bar{u}}_x(\bar{x}_f^+)[1-\phi(\bar{x}_f^+)] - \tilde{\bar{u}}_x(\bar{x}_f^-)(1-\phi_m)}{\phi_m - \phi(\bar{x}_f^+)}. \tag{40}$$

Equating the two expressions to obtain

$$\tilde{\bar{u}}_x(\bar{x}_f^+) = (1-\phi_m)\tilde{\bar{u}}_x(x_f^-) \tag{41}$$

forms the boundary condition at the fluid–solid front, since

$$\tilde{\bar{u}}_x(\bar{x}_f^+) = \bar{h}^2\frac{\partial^3\bar{h}}{\partial\bar{x}^3}. \tag{42}$$

In this case $\bar{h}(1-\phi_m)\tilde{\bar{u}}_x(\bar{x}_f^-)$, the volumetric flow of water at the particle front equals the total evaporation from the packed region, which in scaled form is simply the length of the packed region, $\bar{x}_f$.

With an initial profile consisting of a circular arc for $0 \le \bar{x} \le 2$, followed by a constant thickness for $\bar{x} \ge 2$, the film evolves as shown in Figure 5. The shape is driven by the surface-tension-induced pressure gradient associated with the initial condition. Pinning the film at the corner requires the volume fraction of particles in this region to rise dramatically with evaporation, creating a front of close-packed particles when $\phi = 0.64$ at $\bar{x} = 0$. Further evaporation from this close-packed region then pulls fluid and particles from the dispersed region, causing the front to propagate into the remaining dispersion. At $\bar{t} = 0.36$ one half of the region shown in the graphs has reached close packing, whereas uniform unidirectional drying would produce a fluid film with $\phi = 0.62$ everywhere. This clearly shows the importance of the horizontal drying front.

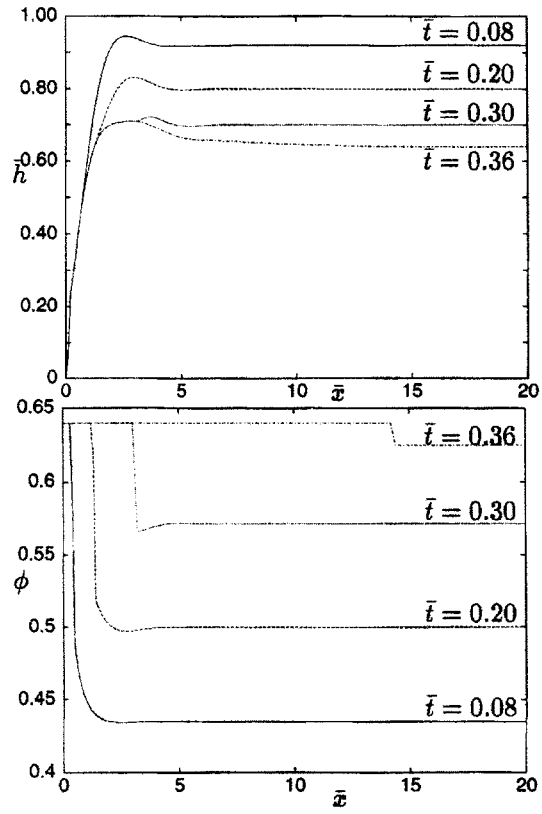

Figure 5. Evolution of height and volume fraction with time with $\bar{p}_{cap} = \infty$, for $\bar{t} = 0.08$ (—); 0.20 (– –); 0.30 (...); and 0.36 (– · –).

The overall rate of evaporation remains constant irrespective of the local volume fraction and height, since the effect of the profile on surface area is $O(H^2/L^2) \ll 1$. Therefore we see inhomogeneous drying rather than any increased evaporation. For a square initial profile, as considered without particles, a front of particles still forms at the edge of the film but propagation is extremely slow. This can be rationalized by an overall particle balance. With a square edge the spatially averaged volume fraction must equal $\phi_0/(1-\bar{t})$. Therefore a front of close-packed particles must be accompanied by an area with volume fraction below the bulk value. In the bulk, where there are no spatial variations in volume fraction, Eqs. 20 and 37 give $\partial\phi/\partial\bar{t} = \phi/\bar{h}$. Therefore the only way to achieve a local depletion in particles is to increase the film height locally above the bulk value of $1-\bar{t}$. At later times the accumulation of material near the edge due to surface-tension-driven flow generated by the initial condition diminishes as evaporation becomes dominant; therefore, propagation of the front slows. With a circular-arc initial condition, the volume fraction can increase above the bulk value without causing a local depletion of particles elsewhere, so propagation is much faster. This is expanded in the subsection on long time approximation.

Receding water fronts at finite capillary pressure

An underlying assumption so far has been that an infinite capillary pressure retains the air–water interface at the film surface and ensures continuing evaporation from all parts of the film. With a maximum for the capillary pressure we expect the interface to recede into the film, thereby reducing the overall rate of evaporation and slowing down the propagation of the front of close-packed particles.

Following Brown (1956), we consider a spherical-cap meniscus in the pore within a triangular array of monodisperse spheres of radius a, suggesting a maximum capillary pressure of around $10\gamma/a \approx 7$ MPa, with $a = 100$ nm. Flow through the packed bed is described by Darcy's law

$$\nabla \cdot \boldsymbol{u} = \mathbf{0} \tag{43}$$

$$-\nabla p = \frac{\mu}{k_p}\boldsymbol{u}, \tag{44}$$

where the permeability, k_p, follows from the Carmen–Cozeny equation (Perry and Green, 1984) such that

$$\frac{dp}{dx} = -\frac{75\mu\phi^2}{2a^2(1-\phi)^2}u_x. \tag{45}$$

For 100-nm radius particles at $\phi = 0.64$, $\mu/k_p = 1.2\times10^{13}$ Ns/m^4. Scaling Eq. 44 as before sets the characteristic pressure as $\mu L^2\dot{E}/k_p H$, and therefore

$$\frac{\partial\bar{p}}{\partial\bar{x}} = -\bar{u}_x \tag{46}$$

$$\frac{\partial\bar{p}}{\partial\bar{y}} = -\left(\frac{H^2}{L^2}\right)\bar{u}_y. \tag{47}$$

So once again the pressure is approximately uniform in the vertical direction.

A water balance at the water–air interface gives

$$\boldsymbol{u}\cdot\boldsymbol{n} = \frac{\dot{E}}{(1+Sk/D_{vap})(1-\phi)}\left[1+\left(\frac{\partial h_w}{\partial x}\right)^2\right]^{1/2} + \frac{\partial h_w}{\partial t}, \tag{48}$$

where $\dot{E}/(1+Sk/D_{vap})$ represents evaporation from a water front receding into a film, as given by Eq. 10, and h_w is the height of the water front at any position. At the water front the pressure is constant at the maximum capillary pressure. Since Eq. 47 specifies the pressure to be uniform vertically, any water front must be vertical, such that $h_w = hH(x-x_w)$, where $H(x-x_w)$ is a step function, and x_w is the position of the water front. Substitution into Eq. 48 relates the velocity of the water front to the evaporation rate and the incoming water velocity $u_x(x_w)$ as

$$\frac{dx_w}{dt} = \frac{\dot{E}}{(1+Sk/D_{vap})(1-\phi_m)} + u_x(x_w), \tag{49}$$

where ϕ_m is the volume fraction at close packing.

Beyond the water front, that is, for $\bar{x}_w < \bar{x} < \bar{x}_f$, integration of continuity (Eq. 43) and substitution of Eq. 48 for the vertical water velocity at the surface of the film gives

$$(1-\phi_m)\frac{\partial}{\partial x}(hu_x)+\dot{E}\left[1+\left(\frac{\partial h}{\partial x}\right)^2\right]^{1/2}=0. \qquad (50)$$

Scaling Eq. 50, invoking the lubrication approximation, and substituting Darcy's law leaves

$$\frac{\partial}{\partial \bar{x}}\left(\bar{h}\frac{\partial \bar{p}}{\partial \bar{x}}\right)=\frac{1}{(1-\phi_m)}. \qquad (51)$$

Integrating this equation twice and setting $\bar{p}(\bar{x}_f)=O(\gamma H/L^2)\ll \bar{p}_{\text{cap}}$ determines the pressure distribution in this packed region as

$$\bar{p}=\bar{p}_{\text{cap}}+\frac{1}{(1-\phi_m)}\int_{\bar{x}_w}^{\bar{x}}\frac{\bar{x}'d\bar{x}'}{\bar{h}} - \frac{(1-\phi_m)\bar{p}_{\text{cap}}+\int_{\bar{x}_w}^{\bar{x}_f}\frac{\bar{x}d\bar{x}}{\bar{h}}}{(1-\phi_m)\int_{\bar{x}_w}^{\bar{x}_f}\frac{d\bar{x}}{\bar{h}}}\int_{\bar{x}_w}^{\bar{x}}\frac{d\bar{x}'}{\bar{h}}. \qquad (52)$$

The velocity at the water front follows as

$$\bar{u}_x(\bar{x}_w)=\frac{(1-\phi_m)\bar{p}_{\text{cap}}+\int_{\bar{x}_w}^{\bar{x}_f}\frac{\bar{x}d\bar{x}}{\bar{h}}}{(1-\phi_m)\bar{h}\int_{\bar{x}_w}^{\bar{x}_f}\frac{d\bar{x}}{\bar{h}}}-\frac{\bar{x}_w}{\bar{h}(1-\phi_m)}, \qquad (53)$$

and Eq. 49 now gives an explicit expression for the motion of the water front with time.

At the particle front Eq. 46 gives an expression for $\bar{u}_x(\bar{x}_f^-)$,

$$\bar{u}_x(\bar{x}_f^-)=\frac{(1-\phi_m)\bar{p}_{\text{cap}}+\int_{\bar{x}_w}^{\bar{x}_f}\frac{\bar{x}d\bar{x}}{\bar{h}}}{(1-\phi_m)\bar{h}\int_{\bar{x}_w}^{\bar{x}_f}\frac{d\bar{x}}{\bar{h}}}-\frac{\bar{x}_f}{\bar{h}(1-\phi_m)}, \qquad (54)$$

that can be substituted in Eq. 42 to form the boundary condition on the remaining fluid. At early times, before the pressure drop along the solid region reaches its maximum value, the water front will not have moved and the evaporation from the packed region equals the length of the packed region multiplied by the evaporation rate, as in the previous example.

Integrating Eqs. 37 and 20 with an initial volume fraction of 0.4 and a circular-arc initial condition as before, but amending the flux boundary condition at the position of the particle front once the water front leaves the edge of the film, as dictated by Eqs. 49 and 53, gives the results shown in Figure 6. Here we ignore the first term in Eq. 49, which represents evaporation from the vertical water front through the dry particles.

Comparing results in Figure 6 with Figure 5 illustrates the effect of the water front in slowing propagation of the particle front. The evolution of the two fronts in Figure 7 reveals the slight movement of the water front before the layer dries, but Figure 8 illustrates that even this small loss of water

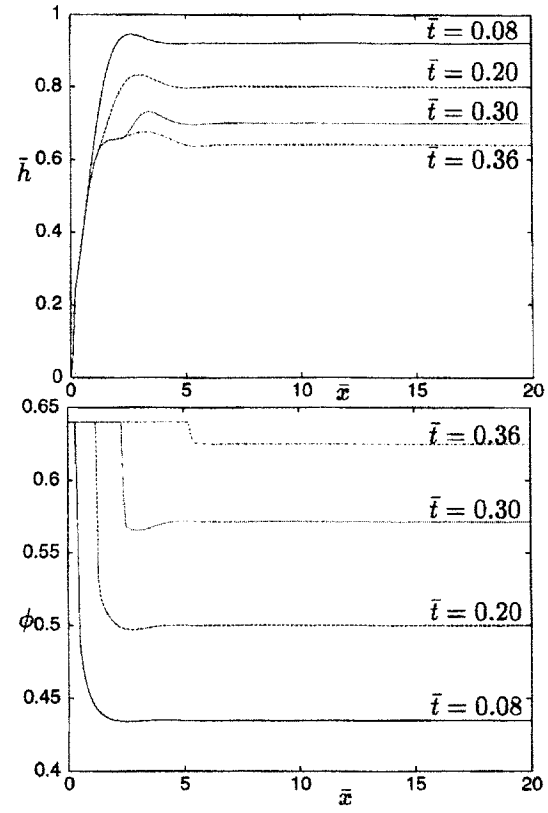

Figure 6. Evolution of height and volume fraction with time with $\bar{p}_{\text{cap}}=1.17$, for $\bar{t}=0.08$ (—); 0.20 (– –); 0.30 (...); and 0.36 (– · –).

amounts to considerable evaporation and retards the progress of the particle front. Figure 8 also demonstrates the acceleration of the particle front as the volume fraction in the bulk film approaches close packing and supports the observations of Winnik and Feng (Winnik and Feng, 1996; Winnik, 1997) that the particle front moves slower with deformable rather than nondeformable particles. Deformed particles would lower the permeability more than the capillary pressure would increase, thereby reducing the dimensionless capillary pressure.

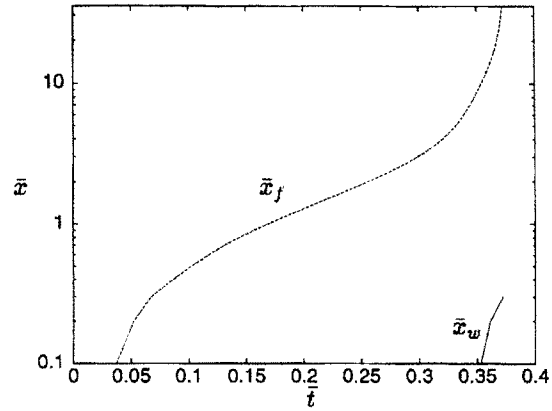

Figure 7. Position of close packed (– –) and water (—) fronts for $\bar{p}_{\text{cap}}=117$.

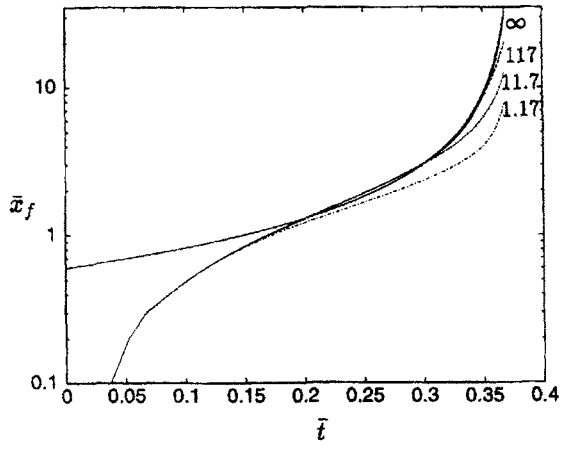

Figure 8. Evolution of particle front with different dimensionless capillary pressures.

$\bar{P}_{cap} = \infty$ (—); 117 (– – –); 11.7 (. . .); and 1.17 (– · –). Line starting at nonzero value is the long time approximation for $\bar{P}_{cap} = \infty$.

Long time approximation

To rationalize the particle-front propagation, we construct an overall solids balance on the film up to the particle front. With an infinite capillary pressure and negligible horizontal flow

$$\phi_m = \frac{\phi_0 \int_0^{\bar{x}_f} \bar{h}(\bar{x},0)\, d\bar{x}}{\int_0^{\bar{x}_f} \bar{h}(\bar{x},0)\, d\bar{x} - \bar{x}_f \bar{t}}, \tag{55}$$

which reduces to

$$\bar{x}_f = \frac{\bar{B}(\phi_m - \phi_0)}{\phi_m(1-\bar{t}) - \phi_0}, \tag{56}$$

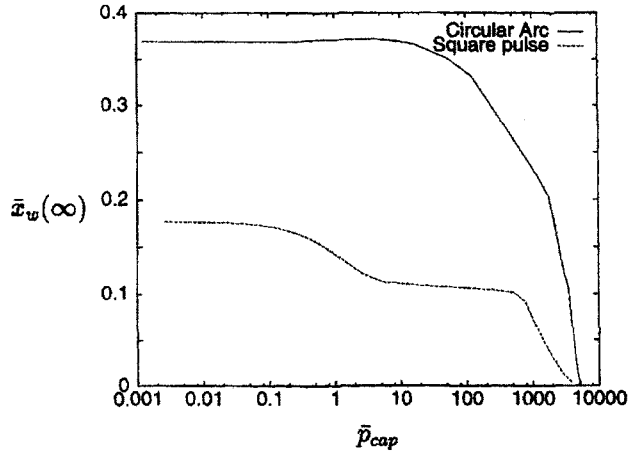

Figure 9. Final recession of water front against dimensionless capillary pressure, for circular arc (—) and square edge (– –) initial conditions.

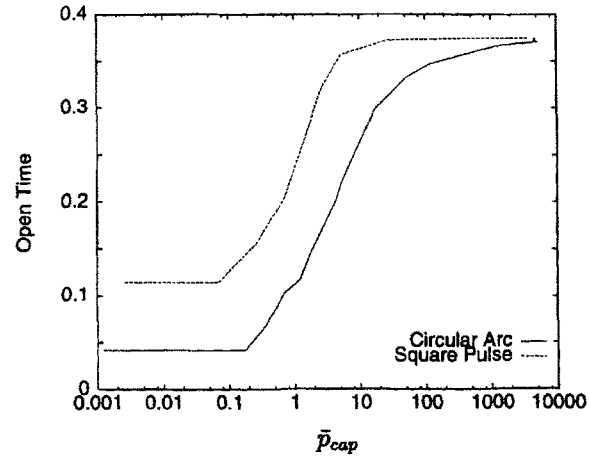

Figure 10. Time before water front moves from edge of film, for circular arc (—) and square edge (– –) initial conditions.

where $\bar{B} = \int_0^\infty [1 - \bar{h}(\bar{x},0)]\, d\bar{x}$. For an initially circular arc between $\bar{x} = 0$ and 2, followed by a flat expanse of fluid, $\bar{B} = 0.602$, so Eq. 56 becomes

$$\bar{x}_f = \frac{0.226}{0.375 - \bar{t}}. \tag{57}$$

This approximation exactly matches the line for infinite capillary pressure in Figure 8. While confirming our numerical analysis, this approximation also shows that the particle front forms entirely because of less fluid at the edge in the initial condition, captured here in the term $\bar{B}$. Thus the effect is quite local, so we expect the position of the particle front for a finite domain to be identical to the infinite domain case.

Total water-front recession and open time

In Figure 9 we plot the total recession of the water front, $\bar{x}_w(\infty)$, against the dimensionless capillary pressure, for two different initial conditions, the lower line being a square shape and the upper line for a circular arc up to $\bar{x} = 2$. As expected the recession falls to zero as the capillary pressure increases. At low capillary pressures the total water-front recession attains a constant asymptote.

In Figure 10 we show the time before the water front leaves the edge of the film, for the same two initial conditions. At low capillary pressures, the water front forms simultaneously with the particle front, which takes almost three times as long with the square edge as with the circular-arc initial condition. At large capillary pressures the water front does not move until the particle front starts to diverge.

The dimensionless capillary pressure,

$$\bar{P}_{cap} = \frac{20}{75}\left(\frac{3\gamma\eta_0}{\dot{E}}\right)^{1/2} \frac{a(1-\phi_m)^2}{\mu\phi_m^2 H}, \tag{58}$$

has the value 2.1×10^4 with the physical parameters estimated previously and $H = 0.1$ mm. This is effectively an infi-

nite capillary pressure, according to Figures 9 and 10. Addition of surfactant to reduce surface tension, use of smaller particles, or a thicker film all reduce $\bar{p}_{cap}$. Thickeners that increase the low shear viscosity will increase $\bar{p}_{cap}$.

Likewise the horizontal length scale, $L = H\,(\gamma/3\eta_0\dot{E})^{1/4}$, decreases if the surface tension is reduced by surfactant or if the viscosity is increased by a thickener and increases with a thicker initial film. Thus smaller particles, thicker films, and low dispersion viscosity always enhance drying at the edge, but the effect of surface tension is not so clear. In the region of $\bar{p}_{cap} \sim 1{,}000$, recession of the water front is such a strong function of $\bar{p}_{cap}$ that a reduction in surface tension is likely to increase the effect.

Since the time scale is $H/\dot{E}(\approx 1$ h), the open time clearly increases with the surface tension, low shear viscosity, and particle size. The effect of the initial film thickness, which affects both the time scale and $\bar{p}_{cap}$, is not clear. The evaporation rate will depend on the relative humidity, as shown by Eq. 10, and the characteristic film thickness on the initial condition, controlled by the film casting. Furthermore, concentration of surfactant in the film as drying proceeds will lead to a time-dependent surface tension. This, along with the increase in low shear viscosity with particle concentration, has been ignored.

Nonuniform Drying

Placing a cover over a film as it dries hinders evaporation. The film height obeys Eq. 20 with evaporation and Eq. 29 without, with the volume fraction governed by Eq. 37 in both cases.

Here we consider spatially periodic evaporation from an initially uniform liquid film, with an infinite maximum capillary pressure. For a period of $50L$ in the horizontal direction with evaporation for $0 \le \bar{x} \le 10$ and $40 \le \bar{x} \le 50$, the final film profile is shown in Figure 11. The film is essentially flat in the evaporating region. At the transition from evaporating to nonevaporating region the film height first decreases and then rises steeply, reaching a maximum at the transition point. A sudden drop is then followed by another steep rise before the surface levels out to a flat film. At the center of the nonevaporating region, the symmetry condition causes the film surface to dip slightly and then rise sharply before dropping dramatically at the center line.

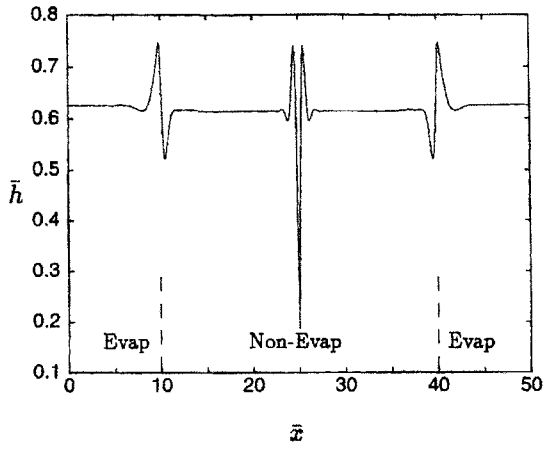

Figure 11. Final height profile for film with evaporation for $0 \le \bar{x} \le 10$ and $40 \le \bar{x} \le 50$.

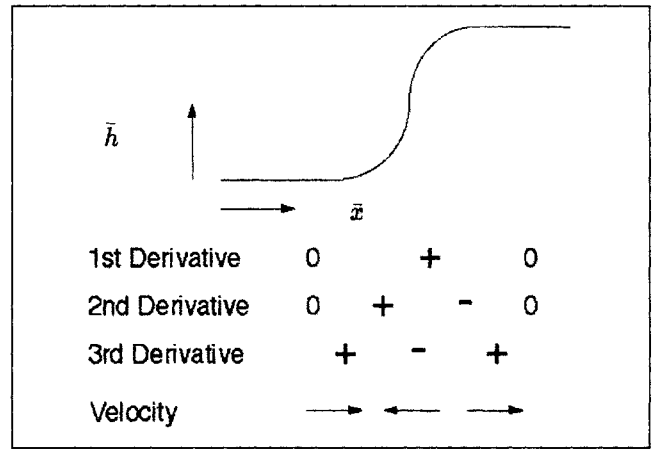

Figure 12. Derivatives of film reduced on one side by evaporation.

The shape at the transition ($\bar{x} = 10, 40$) can be rationalized by considering a flat expanse of fluid, with one half decreasing by evaporation. Initially the fluid surface will be a smooth monotonically increasing curve connecting the two flat halves. The third derivative of such a shape (Figure 12) leads to accumulation of material to the left of the inflection point and depletion to the right, as seen in the final profile. Particle fronts first form at $\bar{x} = 0$, 50 and then move out and through the nonevaporating region. The height of the final film is determined by a balance between the flux of fluid through the moving front of close-packed particles, due to evaporation, and surface tension pushing material ahead of this front. As the particle front nears the center line, the flux of water through the particle front due to continuing evaporation remains roughly constant, but the effect of surface tension in pushing material away is diminished by the no-flux boundary condition at the center. This leads to an increased amount of material at the particle front, causing the rise in the film height there. Near the center line there is a corresponding decrease in the amount of material and the sudden drop in film height.

This situation can be examined experimentally by spreading films on a substrate, so that initially the height is constant everywhere, and selectively hindering evaporation by a cover with regularly spaced holes. The cover sits above the film and at no point is in contact, although it is close enough to hinder evaporation. Figure 13 shows a film produced in this way, with the evaporating regions of 16-mm center-to-center spacing visible as the lighter areas. A magnified view in Figure 14 suggests nonmonotonic variations at the transitions. We estimate the initial film height as 0.15 mm, and from the estimates in the fourth section, determine the center-to-center spacing to correspond to about $4L$. The resulting prediction in Figure 15 illustrates the film height rising from the centers of the evaporating regions on either side up to the transition, and then dropping toward the center of the covered region.

Profilometry (Sloan Dektak Surface Profile Measuring System) provides a quantitative measure of the film profile (Fig-

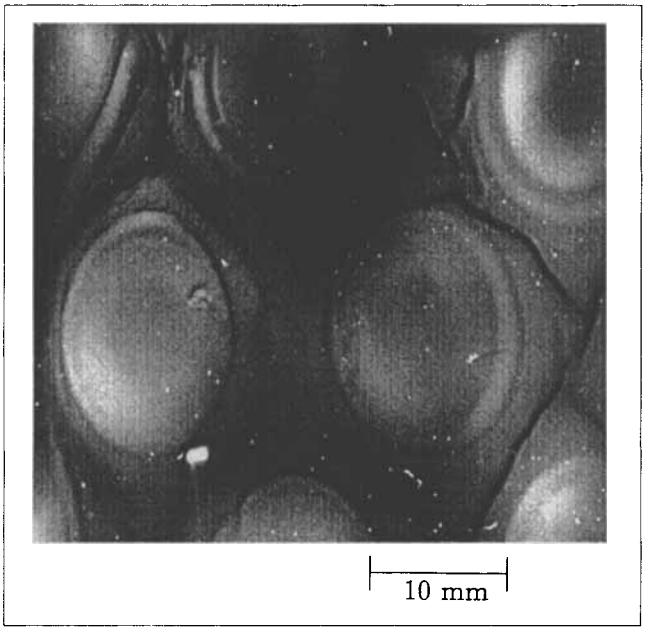

Figure 13. Film with selective evaporation in circular regions.

ure 16) for comparison with Figure 15. The rise in film height from the center of the evaporating region to the transition area and the sudden drop in film height in the nonevaporating region are clearly visible. The drop in the height to the right of the profile corresponds to the edge of the film, chosen to enable the level of the substrate to be shown. The maximum height of the film is approximately 90 μm. Although the similarities between Figures 15 and 16 are striking, only qualitative comparison is possible. The major discrepancy, the apparent size of the evaporative region, is likely to be due to the inability to completely suppress evaporation

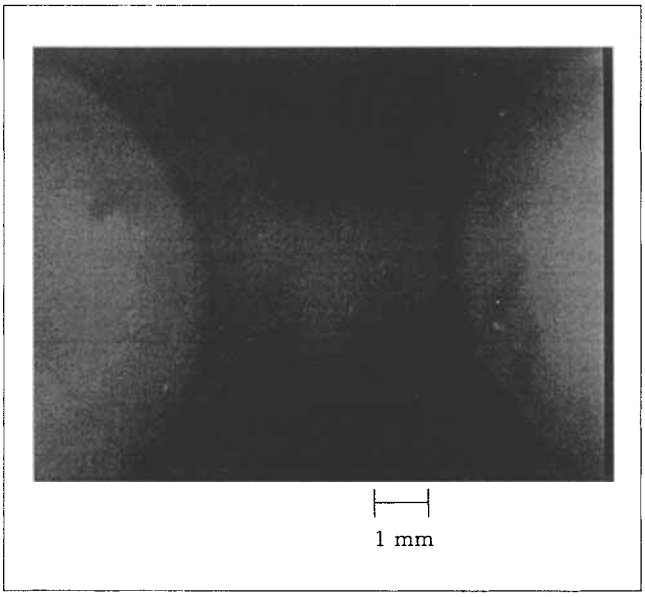

Figure 14. Magnified view of film with selective evaporation in circular lighter regions.

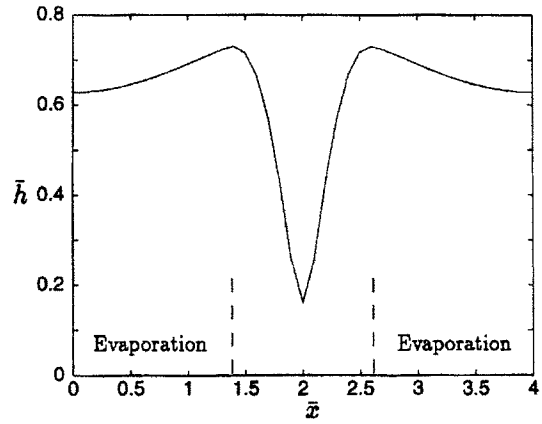

Figure 15. Final film profile with evaporation for $0 \leq \bar{x} \leq 1.4$ and $2.6 \leq \bar{x} \leq 4$.

at the boundaries. Figures 15 and 16 do not show the wild fluctuations seen in Figure 11. The reason is that the experiment only spans a horizontal distance of $4L$, whereas the calculation in Figure 11 covers an expanse of $50L$. Thus in Figures 15 and 16, the separate transition regions at the center and edge of the region with evaporation, in Figure 11, merge to effectively cancel, leaving the depletion at the center, seen in Figures 15 and 16.

Conclusions

We have derived equations governing the flow of evaporating films that are valid in the lubrication limit. With a zero Peclet number in the vertical direction ensuring vertical homogeneity, and an infinite Peclet number horizontally allowing a sudden horizontal change in particle volume fraction, we observe a compaction front that propagates horizontally. Propagation of the front is due to continued evaporation from the packed region, leading to a flux of solvent through the particle front that carries particles along. The velocity of this front can be slowed by a receding water front, which can have a considerable effect without traveling any considerable distance. For the infinite capillary pressure case, the water front does not recede and the position of the compaction front is controlled by the initial condition. The total recession of the water front at the instant the entire film dries is predicted to

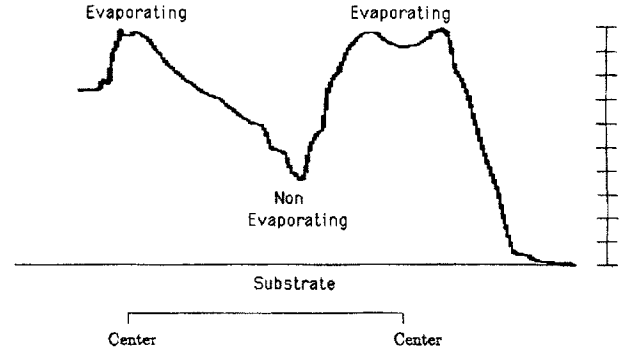

Figure 16. Results from profilometry experiment.

increase with dispersion viscosity, initial film thickness, and smaller particles. The open time before the edge dries is predicted to increase with surface tension, dispersion viscosity, and particle size.

Selective drying of films leads to a final profile that reflects the original region of evaporation. The transition from evaporating to nonevaporating region is marked by a nonmonotonic variation in film thickness, which is supported by the experimental evidence.

Acknowledgments

This research was supported by grants from Rohm and Haas, the Petroleum Research Fund, and a fellowship to A.F.R. from Rhone-Poulenc. The films were prepared by Dr. P. Sperry, Zhenwen Fu, and David Larson at Rohm and Haas.

Literature Cited

Bertozzi, A. L., "Lubrication Approximation for Surface Tension Driven Interfaces: Some Open Problems," *Zamm Z. Angew. Math. Mech.*, **76**, 373 (1996).

Brown, G. L., "Formation of Films from Polymer Dispersions," *J. Poly. Sci.*, **22**, 423 (1956).

Croll, S. G., "Drying of Latex Paint," *J. Coatings Technol.*, **58**, 41 (1986).

Deegan, R. D., O. Bakajin, T. F. Dupont, G. Huber, S. R. Nagel, and T. A. Witten, "Capillary Flow as the Cause of Ring Stains from Dried Liquid Drops," *Nature*, **389**, 827 (1997).

Dillon, R. E., L. A. Matheson, and E. B. Bradford, "Sintering of Synthetic Latex Particles," *J. Colloid Sci.*, **6**, 108 (1951).

Dobler, F., and Y. Holl, "Mechanisms of Latex Film Formation," *TRIP*, **4**, 145 (1996).

Eckersley, S. T., and A. Rudin, "Mechanism of Film Formation from Polymer Latexes," *J. Coatings Technol.*, **62**, 89 (1990).

Frenkel, J., "Viscous Flow of Crystalline Bodies under the Action of Surface Tension," *J. Phys.*, **9**, 385 (1945).

Henson, W. A., D. A. Taber, and E. B. Bradford, "Mechanism of Film Formation of Latex Paint," *Ind. Eng. Chem.*, **45**, 735 (1953).

Keddie, J. L., P. Meredith, R. A. L. Jones, and A. M. Donald, "Kinetics of Film Formation in Acrylic Latices Studied with Multiple-Angle-of-Incidence Ellipsometry and Environmental SEM," *Macromol.*, **28**, 1673 (1995).

Oron, A., S. H. Davis, and S. G. Bankoff, "Long-Scale Evolution of Thin Liquid Films," *Rev. Mod. Phys.*, **69**, 931 (1997).

Overdiep, W. S., "The Effect of a Reduced Solvent Content of Solvent-Borne Solution Paints on Film Formation," *Prog. Org. Coatings*, **14**, 1 (1986).

Overdiep, W. S., "The Levelling of Paints," *Prog. Org. Coatings*, **14**, 159 (1986).

Perry, R. H., and D. Green, *Perry's Chemical Engineers Handbook*, 6th ed., McGraw-Hill, New York (1984).

Russel, W. B., "On the Dynamics of the Disorder-Order Transition," *Phase Transitions*, **21**, 127 (1990).

Sheetz, D. P., "Formation of Films by Drying of Latex," *J. Appl. Polym. Sci.*, **9**, 3759 (1965).

Teletzke, G. F., H. T. Davis, and L. E. Scriven, "How Liquids Spread on Solids," *Chem. Eng. Commun.*, **55**, 41 (1987).

Vanderhoff, J. W., H. L. Tarkowski, M. C. Jenkins, and E. B. Bradford, "Theoretical Consideration of the Interfacial Forces Involved in the Coalescence of Latex Particles," *J. Macromol. Chem.*, **1**, 361 (1966).

Wilson, S. K., "The Levelling of Paint Films," *IMA J. Appl. Math.*, **50**, 149 (1993).

Winnik, M. A., "Latex Film Formation," *Curr. Opin. Colloid Interface Sci.*, **2**, 192 (1997).

Winnik, M. A., and J. Feng, "Latex Blends: An Approach to Zero VOC Coatings," *J. Coatings Technol.*, **68**, 39 (1996).

Manuscript received Oct. 22, 1997, and revision received May 28, 1998.